Accepted Manuscript

Infiltration sintering of WCu alloys from copper-coated tungsten composite powders for superior mechanical properties and arc-ablation resistance

Wenge Chen, Yingge Shi, Longlong Dong, Lijian Wang, Hanyan Li, Yongqing Fu

PII: S0925-8388(17)32893-1

DOI: 10.1016/j.jallcom.2017.08.164

Reference: JALCOM 42921

To appear in: *Journal of Alloys and Compounds*

Received Date: 16 May 2017

Revised Date: 10 August 2017

Accepted Date: 16 August 2017

Please cite this article as: W. Chen, Y. Shi, L. Dong, L. Wang, H. Li, Y. Fu, Infiltration sintering of WCu alloys from copper-coated tungsten composite powders for superior mechanical properties and arc-ablation resistance, *Journal of Alloys and Compounds* (2017), doi: 10.1016/j.jallcom.2017.08.164.

Infiltration sintering of WCu alloys from copper-coated tungsten composite powders for superior mechanical properties and arc-ablation resistance

Wenge Chen[1*], Yingge Shi[1], Longlong Dong[1*], Lijian Wang[1],

Hanyan Li, Yongqing Fu[2, *]

[1] School of Materials Science and Engineering, Xi'an University of Technology, Shaanxi Xi'an, 710048 P.R. China

[2] Faculty of Engineering and Environment, Northumbria University, Newcastle upon Tyne, NE1 8ST, UK.

Abstract: W70Cu30(W-30 wt.% Cu) alloys were fabricated using cold pressing and infiltration sintering methods from two types of powders, i.e., mixed copper-tungsten (M-Cu-W) powders and our newly developed copper-coated tungsten composite (Cu@W) powders. Microstructure, mechanical and arc-ablation properties of the W70Cu30 alloys were investigated, and the mechanism of enhanced physical/mechanical properties and arc-erosion resistance of the W70Cu30 alloys was discussed. For the W70Cu30 alloys prepared using the Cu@W powders, their physical properties, including hardness, electrical conductivity and relative density were much better than those prepared from the M-Cu-W powders. The W70Cu30 alloys fabricated from the Cu@W powders were free of cracks, and showed homogenous distributions of W and Cu network structures. Whereas for the alloys prepared from the M-Cu-W powders, segregation of Cu was observed and the segregation size was about 40~100 μm. Characterization of arc-erosion morphologies

* Corresponding author: Professor Wenge Chen
E-mail: wgchen001@263.net (Wenge Chen), donglong1027@163.com (Longlong Dong), richard.fu@northumbria.ac.uk (Richard Yongqing Fu)

of the W70Cu30 alloys prepared with the Cu@W powders revealed the occurrence of evaporation of Cu phase; whereas that of W70Cu30 alloys prepared with the M-Cu-W powders revealed the occurrence of the sputtering of Cu. After arc breakdown for 200 times, mass loss of alloys made using the mixed powders was twice as much as those made using the coated composite powders. Based on the experimental results and theoretical analysis, an arc breakdown mechanism of the WCu-C alloys using the composite powders was proposed which is attributed to the formation of a homogeneous Cu-Cu network structure to uniformly disperse arc energy and dissipate the generated heat, thus prolonging the service life of the WCu alloy contacts.

Key words: Coated composite powders; Infiltration sintering; WCu alloy; Arc erosion; Breakdown morphology

1. Introduction

WCu alloys are widely used as electrical contact materials in high-voltage circuit breakers due to their high melting point, high hardness, low coefficient of thermal expansion (CTE), good arc erosion resistance of W, and remarkable thermal and electrical conductivities of Cu [1-8]. Phenomena of melting/evaporation, or sputtering of contact materials are commonly observed during their services when the high voltage circuit breakers are subjected to breaking current operations. As results, repeated and concentrated arc erosion will lead to the catastrophic failure of electrical contacts [9-11]. With the development of new switches with larger capacities operated at ultrahigh voltages [12], the conventional preparation methods for the WCu alloys cannot meet the strong demands in applications.

Powder metallurgy (PM) technology has widely been used to fabricate WCu composites. However there are large differences in the material properties between W and Cu, and grain coarsening is difficult to prevent during the high temperature PM sintering process. Cu was reported to be leached out from the skeleton of W during the preparation process which leads to Cu segregation and non-homogenous microstructure, thus poor performance of the final products [13-17]. Therefore, it is critical to control the microstructure and overall density of the products through the PM process, and improve the physical, mechanical and functional properties of the final products.

Preparation of high-performance WCu alloys should start with the improved processing techniques of raw powder materials. Various new methods have been proposed to synthesis WCu powders, such as hydrothermal synthesis, co-reduction method [18], mechanical alloying [19, 20], chemical co-deposition, and hydrogen reduction [21]. The above-mentioned methods can effectively prevent segregation of individual components and promote formation of a homogeneous microstructure, however, it is truly challenging to fabricate highly densified WCu composites using these new technologies, simply because of the large differences in physical properties between W and Cu phases.

Coating the composite powders with two different materials has been frequently used by many researchers in advanced powder metallurgy because this method has no limits on shapes and substrates for the fabrication processes [12]. For example, Sunday et al. produced Fe_3O_4 coated Fe powders, and found that coating Fe with

Fe_2O_3 particles can effectively reduce core loss in soft magnetic composites components [22]. Fan et al [23] obtained homogenous Al-Mg microstructures using silver-coated Al-Mg alloy powders by electroless plating process. Park et al [24] prepared core-shell structures of Ag coated Cu powders using wet chemical processes, and found that dendritic Ag-coated Cu powders exhibit large surface areas, excellent conductivity and good oxidation resistance.

We believe that copper can be coated on tungsten powders surfaces to form composite powders, which could be used in the powder metallurgy to achieve much finer microstructure and superior properties of the WCu alloys. ~~As far as we know, there were no previous studies on copper-coated tungsten composites fabricated via low-cost and conventional processes such as thermo-electroless plating process.~~ The arc-ablation properties of the WCu alloys prepared from Cu coated W powders have never been investigated. This is critical as the WCu alloys have been extensively used in electrical contact field, and their arc-ablation properties are critical for their successful application.

In the present work, Cu coated W composite powders were prepared using the method. For comparisons, W-Cu powders processed using simple mechanical mixing were also fabricated. Then WCu alloys were synthesized using an infiltration process with the above mentioned two types of powders (i.e., mechanical mixed powders and chemical-coated powders). Finally, the mechanical and arc-ablation properties of these two types of WCu alloys were investigated and the arc-erosion mechanisms were discussed.

2. Experimental procedure

2.1 Raw materials

Commercially available tungsten powders (with an average particle size of 5~7 μm, oxygen content ＜600 ppm, purity ≥ 99.9%) and electrolytic copper powders (particle size 48 μm, purity ≥ 99.9%) were purchased from Zhuzhou Cemented Carbide group Co., Ltd, Hunan, China. The detailed information of the chemicals is listed in Table 1. All the other chemicals were obtained from Sinopharm Chemical Reagent Co. Ltd., Shanghai, China.

2.2 Synthesis of Cu-coated W composite powders

As shown in Fig. 1, Cu-coated W composite powders were prepared using the thermo-electroless plating method. The compositions of plating solution and reaction conditions are listed in Table 2. Before the electroless plating process, the W powders were successively etched using solutions of HCl (37 wt.%) and NaOH (30 wt.%) for half an hour successively, and then washed using deionized water.

The detailed electroless plating processes are listed as follows. (a) Copper sulfate, stabilizing agent and complexing agent were mixed together to form an electroless plating solution (see Fig. 1(a)); (b) A certain amount of W powders were added into formaldehyde solution (HCHO) until the surfaces of W powders were thoroughly wetted, then were poured into the electroless plating solution (as shown in Fig. 1(b)); (c) The mixed solution was intensively stirred using a magnetic stirrer to disperse the W powders at 50 °C for 40 min, and simultaneously the NaOH solution was dripped inside the solution to adjust the PH value between 4 to 7 (see Fig. 1(c)); (d) The precipitates were separated from the solution after the chemical reactions were completed (see Fig. 1(d)). Deionized water and concentrated hydrochloric acid were

used to wash the precipitates for several times; (e) The composite powders were then heat-treated at 300 ^{o}C under H_2 atmosphere to re-produce Cu which is coated on W powder surface (Fig. 1(e)). The pH value in the bath was continuously measured using a pH monitoring instrument, and was maintained by adjusting the added NaOH solution using a peristaltic pump. The temperature during electroless plating process was controlled using a constant temperature water bath. After electroless plating process, the Cu-coated W composite powders were then washed using deionized water for more than three times and dried using a vacuum freezed drying machine.

2.3 Property measurement and microstructure characterization

Tungsten-copper mechanical mixed powders (M-Cu-W for a short name, with average particle sizes of W 6~8 μm) and copper coated tungsten powders (Cu@W for a short name with an average particle size of coated powder 12~14 μm) were chosen to fabricate bulk W70Cu30 alloys using the infiltration sintering at 1350 ^{o}C for 90 min under H_2 atmosphere. The detailed preparation process was reported in our previous study [25]. The hardness of W70Cu30 alloys was measured using a TUKON 2100 Vickers micro-hardness tester with a load of 100 g and a dwell time of 20 s. The density of sample was studied using the Archimedes' method. D60K digital conductivity meter was used to examine the conductivity of W70Cu30 alloys by measuring 3~5 points on the same sample to obtain the average value. The thermal diffusivity(α) was measured by using TC3020L at room temperature. The thermal conductivity (κ) was calculated from the relationship(1).

$$\kappa = c\rho\alpha \qquad (1)$$

where c and ρ are specific heat capacity and actual density of the composite,

respectively.

In order to measure breakdown field strength and arc ablation rate during the make-and-break of the contacts, the tests were carried out in the simulator of HYJH-YY/20 kV high voltage switching equipment as shown in Fig. 2. A cylindrical WCu alloys specimen with dimensions of Φ14mm×5mm was polished along the cross-section direction into a mirror surface and used as the cathode, and a W needle was used as the anode. The cathode was slowly moved up with a speed of 0.2 mm/min, and the arc was ignited by the charge breakdown through the gap when the electrode distance was smaller than 1 mm. A direct current (DC) voltage of 18 kV was applied. The breakdown field strength can be obtained using equation (2):

$$E = \frac{U}{d} \tag{2}$$

where E is the breakdown field strength (V/m), U is the breakdown voltage (V), and d is the distance between the cathode and anode (m).

The arc ablation/erosion tests were performed in a chamber with SF_6 atmosphere and the arc erosion rate was determined by the mass loss of the WCu sample. The arc ablation experiments were repeated for 200 times. When the arc was generated between cathode and anode, the arc distance was estimated using a digital micrometer (3101-25AC). The microstructure characterization after electrical breakdown was performed using a scanning electron microscope (SEM) equipped with an energy dispersive X-ray spectrum analyzer (EDS).

In this work, for simplicity, the alloy prepared using the Cu@W composite powders was named as WCu-C, whereas the alloy prepared using the M-Cu-W

powders was named as WCu-M.

3. Results and discussions

3.1 Preparation of Cu@W composite powders

Fig. 3 shows the morphologies of pure W powders and Cu@W composite powders. It can be seen from Fig. 3(a) that the surface of pure W powder (with average sizes of 6-8 μm) is clean, smooth without contaminants. The polyhedral structures of W particles were also clearly observed. However, some W particles show aggregation phenomena due to their larger specific surface areas. Fig. 3(b) shows that surface of Cu coated W particles appears some contaminants and W particles are nearly spherical after thermo-electroless plating. The crystal size of the W powders has been increased (8-12 μm) after the electroless plating process, and the morphology shows that the Cu were successfully coated on the W particle surface. The cross-section image of the coated powder is shown in Fig. 3(c). It can be clearly observed that Cu phase is uniformly coated on the surface of W particles, with the coating thickness in the range from 4-8 μm. Also some porosity were observed arounding coating, which is due to poor interficial bounding between W and Cu. It indicated that some Cu@W powders are not fully covered.

The electroless plating process could happen on the catalytic surfaces at certain pH value and temperature. The electroless Cu deposition process with the formaldehyde as reduction agent can be written using the following reaction:

$$Cu^{2+}+2HCHO+4OH^{-} \longrightarrow Cu+2HCOO^{-}+2H_2O+H_2\uparrow \quad (3)$$

The above reaction is composed of oxidation of formaldehyde and the reduction

of copper ions. The oxidation of formaldehyde is usually a catalytic reaction which occurs in the presence of catalytic metals such as Au, Pd, and Cu. In this work, W powders were coated with Cu, thus without a need to have the catalytic metals, indicating that the deposited Cu could effectively act as the catalytic agent. The Cu thickness was increased and the grain size of the deposited Cu layer was also increased with the reaction time.

Fig. 4 shows the XRD patterns of WCu composite powders. It can be seen from Fig. 4(a) that except the Cu and W, there are also obvious CuO peaks in the diffraction peaks of Cu@W without reduction. This is because that powders were washed and dried at 80 ^{o}C for 12 h under air atmosphere after electroless plating. The surface of the Cu particles can easily be oxidized to CuO in the long-term exposure to the air. Only W and Cu diffraction peaks were observed in Fig. 4(b), which indicated that CuO could be completely reduced at 300 ^{o}C under H_2 atmosphere. Comparing Fig. 4(b) with Fig. 4(c), it can be seen that W peak of Cu@W powders is lower than that of M-Cu-W powders, which is due to the fact that the surface of the W particles is covered by Cu.

3.2 Microstructure of W70Cu30 alloys

Microstructures of W70Cu30 alloys fabricated using the infiltration sintering method are shown in Fig. 5, in which the gray-white particles are W phase and the black ones are Cu phase. It can be seen from Fig. 5(a) that the Cu phase has a certain segregation in the WCu-M alloys (denoted by red arrow in Fig. 5(a)). The Cu are distributed among the W particles and the size distribution is varied in a range of

40~100 μm. In contrast to that, in the WCu-C alloy, the W powders are distributed homogeneously and no obvious Cu or W agglomerates can be observed as shown in Fig. 5(b). Fig. 5(c) and (d) shows the fracture morphology of the W70Cu30 alloys. As can be seen from the images, the network structure of Cu phase was formed and throughout the composites. There are some pores at the junction of W particles and Cu network (denoted by red arrow) in Fig. 5(c). While a small amount of pores were also observed in Fig. 5(d), the bonding phase of Cu fully covered the surface of W particles, indicating that bonding strength between W and Cu is strong. The above analysis shows that Cu@W alloy is more evenly distributed, and the interface connection of W particles and Cu network is stronger than that of M-Cu-W alloys.

In order to explain the microstrutural differences before the sintering, the morphologies of green compacts of WCu-M alloy and WCu-C alloys were characterized and the results are shown in Fig. 6. Comparing Fig. 6(a) with Fig. 6(b), the distribution of W and Cu particles is extremely uneven in the WCu-M green compact, and a number of holes can be observed. However for the coated WCu-C powder structures, few pores could be observed on the green powder surface, as shown in Fig. 6(b). This is understandable because the W particles are uniformly coated by the Cu layer after electroless plating process, and this special structure makes the formation of Cu-Cu contacts preferentially instead of that of W-W contacts during the fabrication process. Additionally, the good plastic deformation of Cu can effectively reduce the arch bridge effect caused by direct contact of W particles, thus the porosity is significantly reduced. The binder Cu phase can lead to the

rearrangement of W particles, thus achieving the closest packing density. The initial point- or small area contacts among particles are gradually changed into the atomic bonding through the heating, volume diffusion, grain boundary diffusion of material migration during the infiltration sintering process, thus resulting in a densified structure. W particles are distributed homogeneously in the coated powders, and the number of W particles in contact with each other is much higher.

For WCu-C alloys, the distance of material transfer during sintering is obviously shortened during the sintered neck formation, leading to formation of a continuous W skeleton. Simultaneously, the melted Cu liquid can be adequately immerged into compact pores under the capillary force, and Cu phase is distributed around the W skeleton forming a network structure.

3.3 Physical and mechanical properties of W70Cu30 alloys

Physical and mechanical properties of the W70Cu30 alloys made of different powders are listed in Table 3. It can be seen from Table 3 that both the alloys of WCu-C and WCu-M meet the requirements of the industrial Standard (GB/ T8320-2003). Whereas the properties of WCu-C alloy are much better than those of the WCu-M one. The reason for the relatively inferior properties of WCu-M alloys is due to the uneven distribution of W and Cu and the large difference in density of W (19.36 g/cm^3) and Cu (8.96 g/cm^3). In addition, the network structure of Cu phase and less porosity are very important for the excellent conductivity and thermal conductivity of WCu alloys [26]. These problemes can be solved by using core-shell structures of the WCu-C composite powders, as seen in Fig. 3(c) and Fig.5(d).

Therefore, the electrical and thermal conductivities of the alloys can be improved by the core-shell structures. Moreover, the Cu layer coated onto the W particles can play a good lubrication role during the following molding/demolding processes, so that the W particles can be ~~easily deformly and~~ moved to realize full contacts among W and Cu particles, thus reducing the porosity of the green compacts. Accordingly, during the sintering process the wettability between W skeleton and Cu molten particles can be improved by using the WCu-C powders. Therefore, the molten Cu would be thoroughly immerged into the W skeleton (as shown in Fig. 6(b)). As a result, the physical and mechanical properties of the WCu-C alloy can be significantly enhanced. Whereas for the WCu-M alloy, the relatively poorer performance is mainly due to the uneven distribution of W phase and Cu phase in the sintered alloys.

Due to the immiscibility of solutions between Cu and W, the densification of WCu composites mainly occurs during solid-state sintering which is strongly influenced by the homogeneity and sinterability of W and Cu powders. When the W and Cu powders are mixed together, the initial density of the WCu composites is quite low, and this is mainly because the inhomogeneous distributions of W and Cu powders produce many pores which inhibit the mass transport of the Cu and W atoms. It is well- known that it is rather difficult to homogeneously mix W and Cu powders due to the large differences in the densities of W and Cu. During sintering process, many W powders agglomerate together, thus generating the bridge effect, however, Cu powders are difficult to fill inside these pores. Whereas if the Cu-coated W powders are used, the high relative density of WCu composites can be achieved due

to the formation of homogeneously distributed W powders and improved sinterability of the composite powders. As the W powders are coated with Cu forming a core-shell structure, the bridge effect between W powders can be eliminated to reduce pores in the compact of WCu composites. During the heating stage in the sintering, the Cu diffuses easily on the surfaces of the composite powders, thus resulting in the necking effect. The composite powders are easily sintered together with growth of rapid Cu necking effects, thus the mass transport of Cu and W atoms will be significantly enhanced. ~~It was reported that the activation energy for self-diffusion on the W surface was decreased from 300 to 87 kJ/mol as the W was coated with Ni [27]. Similarly the Cu@W powders are also beneficial to promote the self-diffusion of W atoms.~~ Also the activation energy for self-diffusion Q_{SD} for Cu(Q_{SDCu}=203.6 KJ/mol) on the surface of coated powders were lower than that of W(Q_{SDW}=626.3 KJ/mol)[27], which is benefical to diffision. Thus shortening the time of material migration. This improvement in the mass transport by using the composite powders also leads to the rapid densification of WCu composites. Therefore, both the increased mass transport effect and enhanced sintering mode through self-diffusion of W significantly enhance the densification of WCu composites after sintering. According to above results and analysis, using the Cu@W powders, the densification of WCu composites can be significantly increased, and also the porosity of the WCu composites is also significantly decreased, thus achieving the excellent physical properties of the sintered alloys(as seen in Fig. 5(d)).

3.4 Arc-ablation properties of W70Cu30 alloys

Fig. 7 plots the relationship between the mass loss and arc breakdown times of W70Cu30 alloys. Clearly there are three stages during the arc ablation process of the WCu-M alloy. The first stage is before 80 times breakdown (□), and the relationship between the mass loss and breakdown times showed a linear increasing trend. After this stage (□), with the further increase in the breakdown times, the mass loss of the alloy is gradually reduced, thus reaching to the steady stage of the arc ablation (□). It was reported that the lifetime of the contact material depends on this critical stage [28]. In the third stage, the mass loss increases constantly, and the mass loss reaches 0.6 mg after arc breakdown for 200 times (□). For the WCu-C alloy, its trend is similar to that of WCu-M alloy, and the apparent differences are: (1) there is a much longer second stage (up to 160 times); and (2) the mass loss is much less after the same repeated breakdown times.

In the initial stage, the mass loss of both the two types of W70Cu30 alloys is quite large because some burrs and other oxide are inevitably existed on the surface of alloy. They are easily subjected to arc breakdown, and local heating or ion sputtering can be generated, thus resulting in the rapid removal of those attachments on the surfaces, which was often called old-refine stage [5]. However, the mass loss increases after this as the removed W and Cu vapors would react with SF_6 (an arc-extinguishing medium) at the high arc temperature, the main recation is shown in equation (4), leading to formation of metal fluorides, which are attached to the surface of the alloy.

$$\left.\begin{aligned} &3SF_6 + W \rightarrow WF_6(g) + 3SF_4(g), \\ &SF_6 + Cu \rightarrow CuF_2(s) + SF_4(g), \end{aligned}\right\} \quad (4)\ [29]$$

$4SF_6 + 3W + Cu \rightarrow 2S_2F_2(g) + 3WF_6(g) + CuF_2(s)$

The ablation products of the WCu-C and WCu-M alloy were examined using the EDS. Results show that there are F and S elements but not W and Cu element as shown in Fig. 8, which clearly proves the above assumptions.

The steady ablation stage of the WCu-C alloy is much longer than that of WCu-M one, and the ablation mass loss is much less. These are mainly due to the formation of network microstructures for the WCu-C alloy, which is efficient to conduct the heat transfer [30]. Therefore, most of heat generated by the arc ablation can be quickly transferred out. Also, much finer and more homogeneous distribution of Cu phases in the alloys is in favor of uniform distribution of arc charging. Accordingly the arc energy per unit area becomes much smaller and the breakdown field strength of the WCu-C alloy (4.22×10^6V/m) is higher than that of the WCu-M alloy (3.78×10^6V/m). With further increase of the arc breakdown times, the Cu content on the surface becomes rapidly lost, and part of W particles were exposed, leading to the decrease the bonding strength of W and Cu phases. The pores also appear collapsed and the ablation weight loss of the W70Cu30 alloy is significantly increased due to the arc breakdown. This is the failure mechanism of the contact materials in the last stage.

The surface morphologies of the W70Cu30 alloy after the first arc breakdown in the SF_6 (extinguished medium) is shown in Fig. 9. A circular arc erosion region with a diameter of 220~230 μm can be observed on the surface of WCu-C alloy. The ablation region is smooth, and some sprayed products are appeared on the ablation center (as

shown in arrow in Fig. 9(a)). EDS analysis showed they are mainly Cu element with a small quantity of W element, which may be attributed to the arc preferential breakdown on the lower work function of Cu phase during arc ablation process.

Comparing Fig. 9(a) with Fig. 9(b), it can be concluded that the ablation area of the WCu-M alloy are much smaller than that of the WCu-C one. In addition, a molten region was formed in the process of arc action, and the liquid droplets of copper were sprayed out from the molten region under the arc force then they were quickly solidified and deposited on the surface, thus forming many tiny bumps and leading to a rough surface. The above results reveal that the arc breakdown on the surface of WCu-M alloy is more concentrated and the arc is mainly focused in the copper segregation region, which can explain the formation of copper spraying and evaporation. Finally, the ablation craters were formed in these positions as shown in the arrows in Fig. 9(b). Similar phenomena have been reported in Ref [11]. However, this phenomenon was not observed in the WCu-C alloy due to its finer and more uniform distribution of Cu phase. Under the same condition, arc energy of per unit area in the WCu-C alloy is much less, and the ablation morphology is much less significant. It is believed that a uniform distribution of Cu phases play an important for uniformly dispersing the arc energy throughout the whole area. Of course, the high electrical and thermal conductivity of composites can not be ignored. For WCu contacts materials, the conductivity of composite is higher, and its anti-ablation is stronger. Because good conductivity or thermal conductivity can quickly spread the heat generated by the arc, avoiding the alloy contacts to withstand excessive heat

ablation.

Fig. 10 shows SEM morphologies of the W70Cu30 alloys after arc breakdowns for 200 times. Comparing Fig. 10(a) and Fig. 10(c), it can be found that a certain ablation regions are formed on the surfaces of WCu-C and WCu-M alloys after arc breakdowns 200 times, and the ablation areas in Fig. 10(a) is much smaller than that in Fig. 10(c). In Fig. 10(a), the ablation surface is much smoother without obvious ablation defects, whereas in Fig. 10(c), the surface is relatively rough with some bumps and ablation holes existed on the surface. This clearly indicates the severe loss of materials in the WCu-M alloy under the repeated arc action. The differences in the morphologies after multiple breakdowns between WCu-C and WCu-M alloys are mainly caused by the differences in the uniformity of microstructure distribution.

Of course the influences of the ablation morphology after the first breakdown on the subsequent breakdown processes should also significantly influence the morphologies. According to the previous analysis shown in Fig. 9(b), lots of bumps are appeared on the WCu-M alloy after the first arc breakdown. The electric field strengths of these bumps are increased dramatically compared with that of the smooth substrate surface under the strong electric filed. The tips of these bumps are suffered a concentrated electric field, thus their field emission strength are increased to generate new arc breakdown. With the increase of the breakdown times, even though some bumps disappear due to the arc ablation, the other bumps in a larger area could generate new arc breakdown, thus resulting in a much larger ablation area than that of the WCu-C alloy.

Comparing Fig. 10(b) and Fig. 10(d), it is clear to see the cumulative effect of multiple breakdowns in the ablation area for both the WCu alloys. The arc breakdowns are mainly focused in the Cu segregation regions of the WCu-M alloy, whereas there is no obvious such type of region for the WCu-C alloy. The deposition of the Cu phases can also be observed in both Figs. 10(b) and 10(d). A large amount of Cu droplets are observed to attach to the W particles in Fig. 10(b), whereas only a small amount of Cu droplets are observed to attach to W particles as shown in Fig. 10(d).

Results clearly reveal that there are significant differences in the residual amounts of Cu phase on the surface layers of two types of alloys and the arc-erosion process during the arc breakdowns. The dominant arc-erosion mechanism of WCu-C alloy is the evaporation of Cu phase, which can be manifested by the large amount of Cu phases observed on the surface layer and the finer and more uniform of deposited Cu particles. The erosion morphology from the multiple arc breakdowns occurs on a much larger area of the surface than that on the first arc breakdown.

However, for the WCu-M alloy, the arc-erosion mechanism is mainly the sputtering of Cu phase, in which Cu instantly becomes Cu vapour under the high arc temperature thus bursting and generating large pressure. As shown in Fig. 10(d), there is an ablation crater with a diameter of 80~100 μm observed on the ablation region, whose surrounding microstructures are not having a large stress. The loss of Cu phase occurs not only on the surface, but also inside the alloy. In addition, some cracks can be observed around the ablation crater, which are formed mainly by the large thermal

stresses caused by the large differences in the CTEs of the W and Cu (CTE_{Cu} =17.5 × 10^{-6}/K, CTE_W = 4.6 × 10^{-6}/K) [31]. ~~as well as the large internal stresses produced in the sintering and solidification processes.~~ The thermal mismatch between Cu and W results in large thermal stress within composites as cooling from arc ablation temperature to room temperature. When the thermal stress is higher than the interfacial bonding strength between Cu and W, it will produce gaps at the interfaces of Cu and W.

3.6 Discussions on the arc breakdown mechanisms for W70Cu30 alloys

In order to explain the phenomena observed in the present work and to further understand the principles and mechanisms, a schematic model is plotted in Fig. 10 to explain the arc ablation phenomena occurring on the W70Cu30 alloy surface. As is known, surface ablation processes mainly include thermal chemical reaction of surface material and ambient air flow, material melting, evaporation (sublimation), high velocity particle impact (erosion) and mass loss caused by mechanical erosion [32].

For the WCu-M alloys, W skeleton phase is prone to launch electrons because the work function of Cu is less than that of W. Hence the selective arc breakdown should take place on the surface of W phase under the action of arc. However, Cu phase was molten instantaneously since the melting point of Cu is three times lower than that of W. At the same time, the Cu phase is partially clustered and uneven (In Fig. 10(a) and (c)), which result in a large area of pits and craters, as shown in Fig. 9(c) ~ (d).

Whereas for the WCu-C alloys, Cu is uniformly coated on the surfaces of W particles to form Cu-Cu interconnecting network skeleton, as shown in Figs. 10(b) and (d). Therefore, the arc movement of sample surface is different from that on the WCu-M alloys, which could be described as follows. When the arc breakdown occurs, copper cladding can restrain the electron emission, also the generated heat can be quickly dissipated inside the homogeneous Cu-Cu network structure and also released by evaporation of Cu. At the same time, the arc energy is uniformly dispersed on all the Cu@W particles, then multiple weak arcs will be easily generated and quickly dispersed under the action of the strong electric field (Fig. 10(d)). The arc energy distributed on each Cu@W particle is significantly reduced. Subsequently, the temperature of arc breakdown zone could be significantly reduced through heat transfer by the connected Cu-Cu skeleton, thus avoiding the generation of splashed molten droplets of Cu. When the arc breakdown happens again, the formation of the secondary spots is relatively easier due to the uniform distribution of the weak Cu phases. So the whole surface of the WCu-C alloys have the equal chance of arc breakdown in all directions, and the cathode spots are uniformly distributed in all directions on the surface, thus resulting in the morphologies shown in Figs. 9(a) ~ (b). On the other hand, the electron emission was suppressed due to low function of Cu coated on high function of W, delaying the high temperature generation from the arc. As a result, the splash of liquid Cu was reduced effectively, thus improving arc stability, prolonging the life of W70Cu30 alloys contact.

4. Conclusions

In this work, the arc-erosion properties and mechanical properties of the W70Cu30 alloys prepared using both W-Cu mechanical mixed powders and copper coated tungsten powders have been investigated. The following conclusions can be drawn from the present work:

(1) The microstructures of the W70Cu30 alloy prepared using the coated composite powders are more uniform and finer, with a homogenous W skeleton formed in the alloys. However, the Cu phase in the simple mechanical mixed powder has a certain segregation which appeared to be strip-like shape with the size of 40-100 μm.

(2) The hardness, density , electrical and thermal conductivity of the WCu alloys using the coated powders fabrication are all excellent than that of obtained using the mixed powders.

(3) The arc-erosion resistance of the WCu-C alloy is better than that of WCu-M alloy. For the WCu-C alloy, the ablation area was larger and the ablation crater was shallower, and the arc erosion is mainly attributed to the evaporation of the low melting point Cu. However, for the WCu-M alloy, the arc erosion was mainly due to the sputtering of Cu. After arc breakdowns 200 times, the ablation morphology was serious and the mass loss was 0.6 mg, which was 2 times as much as those of the WCu-C alloy.

(4) The arc breakdown mechanism of WCu-C alloys was considered to be the formation of a homogeneous Cu-Cu network structure to disperse arc energy and dissipate heat, thus prolonging the service life of the WCu contacts.

Acknowledgements

The authors would like to acknowledge the financial support from Key Research and Development Projects of Shaanxi Province **(No. 2017ZDXM-GY-050)** and the Technological Innovation Research Funds of Xi'an, Newton Mobility Grant (IE161019) through Royal Society and the National Natural Science Foundation of China, and Royal academy of Engineering UK-Research Exchange with China and India.

Reference

[1]. L.J. Kecskes, B.R. Klotz, K.C. Cho, R.J. Dowding, M.D. Trexler, Densification and structural change of mechanically alloyed W-Cu composites, Metall. Mater. Trans. A. 32(2001): 2885-2893.

[2]. A. Ibrahim, M. Abdallah, S.F. Mostafa, A.A. Hegazy, An experimental investigation on the W–Cu composites, Mater. Des. 30(2009): 1398-1403.

[3]. K. Sebastian, High-density tungsten-copper liquid phase sintering composites from coreduced oxide powders, Int. J. Powder. Metall. 15(1979): 45-53.

[4]. X. Yang, S. Liang, X. Wang, P. Xiao, Z. Fan, Effect of WC and CeO_2, on microstructure and properties of W-Cu electrical contact material, Int. J. Refract. Met. Hard Mater. 28(2010): 305-301.

[5]. W. Chen, L. Dong, Z. Zhang, H. Gao, Investigation and analysis of arc ablation on WCu electrical contact materials, J. Mater. Sci.: Mater. Electron. 27(2016): 5584-5591.

[6]. H. Gao, W. Chen, Z. Zhang, Evolution mechanism of surface nano-crystallization of tungsten-copper alloys, Mater. Lett. 176(2016): 181-184.

[7]. L. Dong, W. Chen, C. Zheng, N. Deng, Microstructure and properties characterization of

tungsten–copper composite materials doped with graphene, J. Alloy. Compd, 695(2017): 1537-1646.

[8]. L. Dong, W. Chen, N. Deng, J. Song, J. Wang, Investigation on arc erosion behaviors and mechanism of W70Cu30 electrical contact materials adding graphene, J. Alloy. Compd. 696(2017): 923-930.

[9]. Y. Su. W. Chen, X. Zhang, B. Ding, Effect of microstructure of material on arc cathode spot, Rare Metals, 29(2005): 495-460.

[10]. X. Wu, Z. Lee, Theoretic analysis on sputter erosion of electrode, Proceedings of the Csee, 23(2003): 96-97.

[11]. X. Wei, D. Yu, Z. Sun, Z. Yang, X. Song, Arc characteristics and microstructure evolution of W-Cu contacts during the vacuum breakdown, Vaccum, 107(2014): 83-89.

[12]. Z. Lu, L. Luo, J. Chen, X. Huang, J. Cheng, Y. Wu, Fabrication of W-Cu/CeO_2 composites with excellent electric conductivity and high strength prepared from copper-coated tungsten and Ceria powders, Mat. Sci. Eng. A, 626(2015): 61-66.

[13]. Q. Zhou, P. Chen, X. Gao, W. Sheng, Experiment study on the hot-shock consolidation of tungsten powder, Mater. Sci. Forum, 673(2011): 107-112.

[14]. L. Duan, W. Lin, J. Wang, G. Yang, Thermal properties of W-Cu composites manufactured by copper infiltration into tungsten fiber matrix, Int. J. Refract. Met. Hard Mater. 46(2014): 96-100.

[15]. F.A.D. Costa, A.G.P.D. Silva, U.U. Gomes, The influence of the dispersion technique on the characteristics of the W-Cu powders and on the sintering behavior, Powder Technol. 134(2003): 123-132.

[16]. M. Ardestani, H. Arabi, H.R. Rezaie, H. Rczavizadeh, Synthesis and densification of

W-30wt% Cu composite powders using ammonium meta tungstate and copper nitrate as precursors, Int. J. Refract. Met. Hard Mater. 27(2009): 796-800.

[17].L. Xu, M. Yan, Y. Xia, J. Peng, W. Li, L. Zhang, C. Liu, G. Chen, Y. Li, Influence of copper content on the property of Cu-W alloy prepared by microwave vacuum infiltration sintering, J. Alloy. Compd, 592(2014): 202-206.

[18].L. Wan, J. Cheng, P. Song, Y. Wang, T. Zhu, Synthesis and characterization of W-Cu nanopowders by a wet-chemical method, Int. J. Refract. Met. Hard Mater. 29(2011): 429-434.

[19].Y. Meng, Y. Shen, C. Chen, Y. Lee, X. Feng, Effects of Cu content and mechanical alloying parameters on the preparation of W–Cu composite coatings on copper substrate, J. Alloy. Compd 585(2014): 368-375.

[20].W. Chen, Z. Kang, H. Shen, B. Ding, Arc erosion behavior of a nanocomposite W-Cu electrical contact material, Rare Metals, 25(2006): 37-42.

[21].J. Lee, W. Chen, W. Tao, F. Shao, B. Ding, Nano-composite powder of tungsten coated copper produced by thermo-chemistry co-reduction, Rare Metal Mat. Eng. 41(2012): 2091-2094.

[22].K.J. Sunday, F.G. Hanejko, M.L. Taheri. Magnetic and microstructural properties of Fe_3O_4 coated Fe powder soft magnetic composites, J. Magn. Magn. Mater. 423(2016): 164-170.

[23].Y. Lee, Q. Wang, M. Shi, Process of electroless silver coated Al-Mg alloy powder, Rare Metal Mat. Eng. 44(2015): 2633-2636.

[24].Y.S. Park, C.Y. An, P.K. Kannan, N. Seo, K. Zhuo, Fabrication of dendritic silver-coated copper powders by galvanic displacement reaction and their thermal stability against oxidation, Appl. Surf. Sci. 389(2016): 865-873.

[25]. B. Liu, W. Chen, Z. Zhang, Tungsten-copper alloy surface nano-crystallization and its

properties, Rare Metal Mat. Eng. 44(12) (2015) 3188-3191.

[26].L. Zhang, W. Chen, G. Luo, P. Chen, Q. Chen, W.Chen, Low-temperature densification and excellent thermal properties of W–Cu thermal-management composites prepared from copper-coated tungsten powders, J. Alloy. Compd, 588(2014):49-52.

[27].K. Edalati, Z. Horita, Correlations between hardness and atomic bond parameters of pure metals and semi-metals after processing by high-pressure torsion, Scripta Materialia, 64(2011):161-164.

[28].K. Tseng, C. Kung, T. Liao, K. Chen, D. Han, Investigation of the arc erosion behaviour of W-Cu composites, Can. Metall. Quart. 49(3) (2010): 263-274.

[29].J.wang, Sulfur hexafluoride decomposition products and removal methods, Organic fluorine industry, 4 (1994): 7-11

[30].W. Chen, J. Ding, Study on electrical life time of W-Cu contacts materials, Electrical material, 3(2003): 21-24.

[31].J. Emsley, The Elements, 2nd ed., Oxford Univ., Oxford. 1991, pp. 56–202.

[32].P.D. Kumar, S. Kumar, R.T. Thakur, A. Upadhyay, T. Raychaudhuri, Erosion and lifetime evaluation of molybdenum electrode under high energy impulse current, IEEE. T. Plasm. Sci. 49(4) (2011): 1180-1186.

List of figure captions:

Fig.1 Illustration of the preparation process of Cu coated W powders via thermo-electroless plating.

Fig. 2 Experiment testing apparatus: (a) the scheme of the testing facility; (b) experimental circuitry diagram of vacuum struck.

Fig. 3 The morphology of copper coated tungsten composite powders (a) Pure tungsten powders, (b) Copper coated tungsten powders, (c) Cross section of the coated powder.

Fig. 4 XRD patterns of (a) Cu@W without reduction, (b) after reduction and (c) M-Cu-W powders.

Fig. 5 Microstructure and fracture morphology of W70Cu30 alloys prepared with (a),(c) M-Cu-W powders, (b),(d) Cu@W composites powders.

Fig. 6 The morphology of W70Cu30 green compacts (a) M-Cu-W powders, (b) Cu@W composites powders.

Fig. 7 The curves of arc ablation times and mass accumulated lost of different W70Cu30 alloys.

Fig. 8 EDS energy spectrum of W70Cu30 alloy arc breakdown under SF_6 gaseous medium.

Fig. 9 The surface microstructure after first arc breakdown of W70Cu30 alloy

(a) WCu-C alloy, (b) WCu-M alloy.

Fig. 10 The surface microstructure after arc breakdown 200 times of W70Cu30 alloy prepared with different powders (a) and (b) WCu-C alloy, (c) and (d) WCu-M alloy.

Fig. 11 Schematic illustration of the vacuum breakdown process for WCu alloys.

List of table captions:

Table 1 Chemical compositions of W and Cu powders (mass fraction, %).

Table 2 The compositions of plating solution and reaction conditions.

Table 3 The Physical and mechanical properties of W70Cu30 alloy prepared with different composites powders.

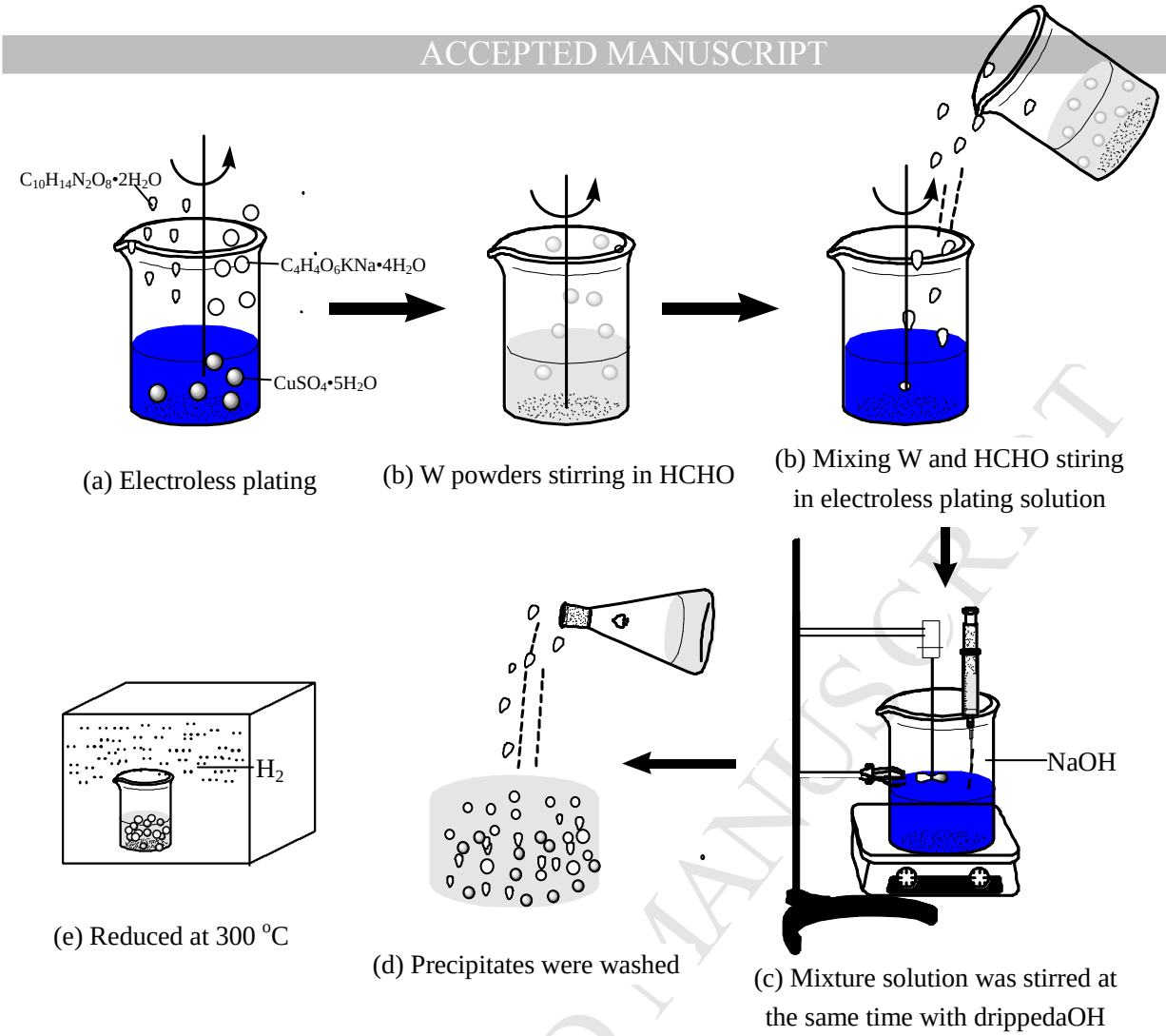

Fig.1 Illustration of the preparation process of Cu coated W powders via thermo-electroless plating.

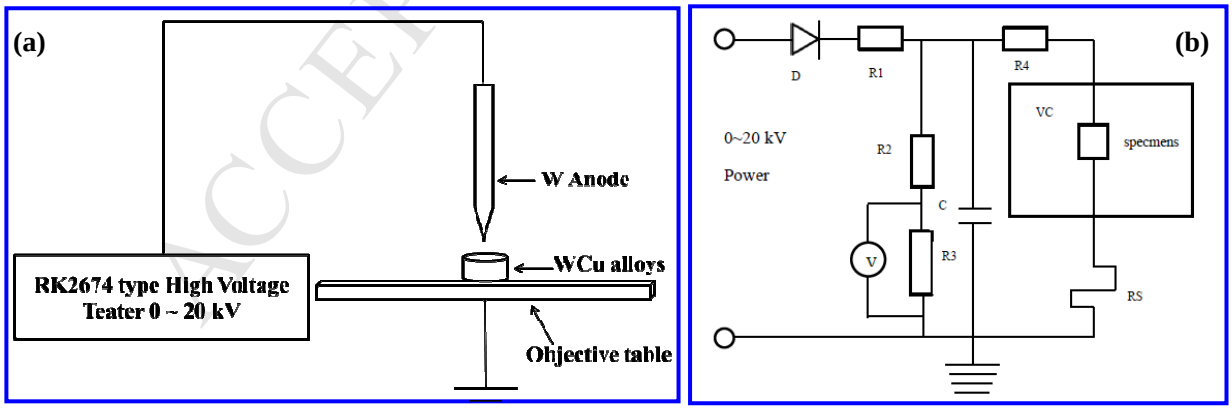

Fig. 2 Experiment testing apparatus: (a) the scheme of the testing facility; (b) experimental circuitry diagram of vacuum struck.

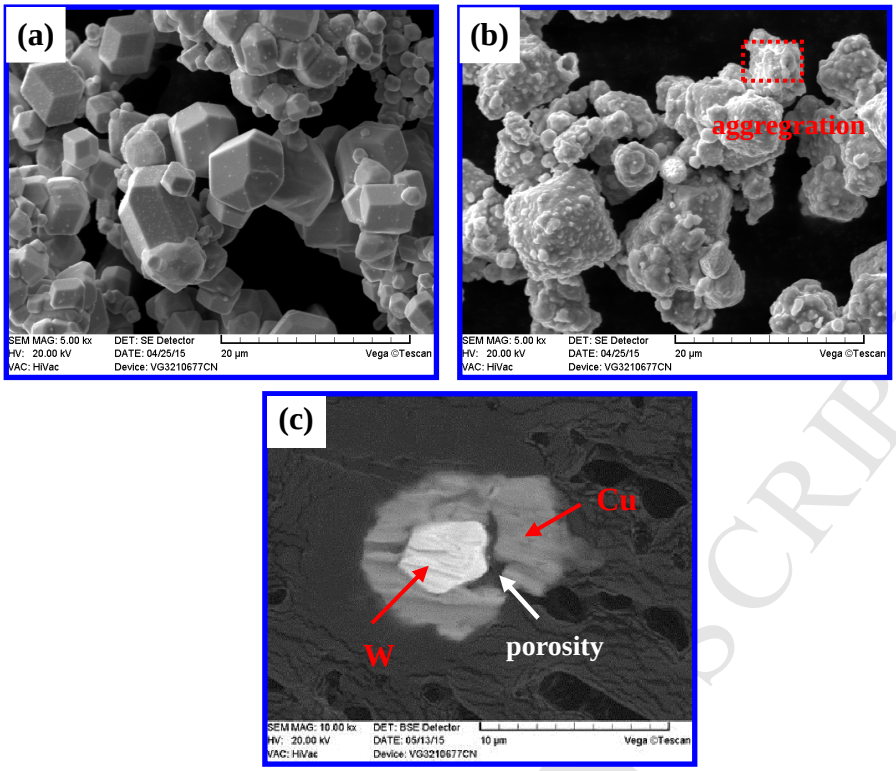

Fig. 3 The morphology of copper coated tungsten composite powders (a) Pure tungsten powders, (b) Copper coated tungsten powders, (c) Cross section of the coated powder.

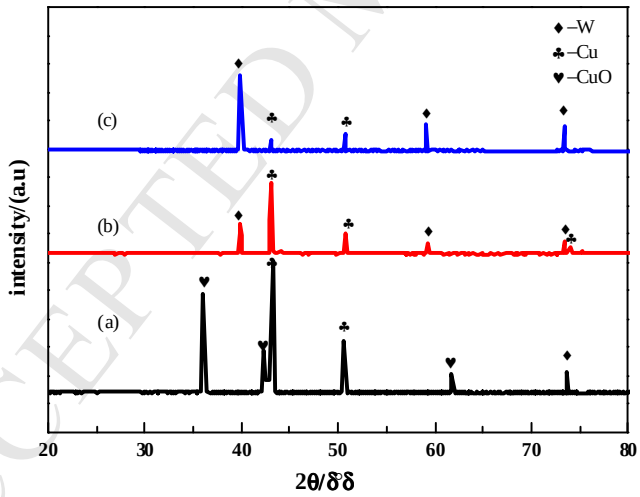

Fig. 4 XRD patterns of (a) Cu@W without reduction, (b) after reduction and (c) M-Cu-W powders

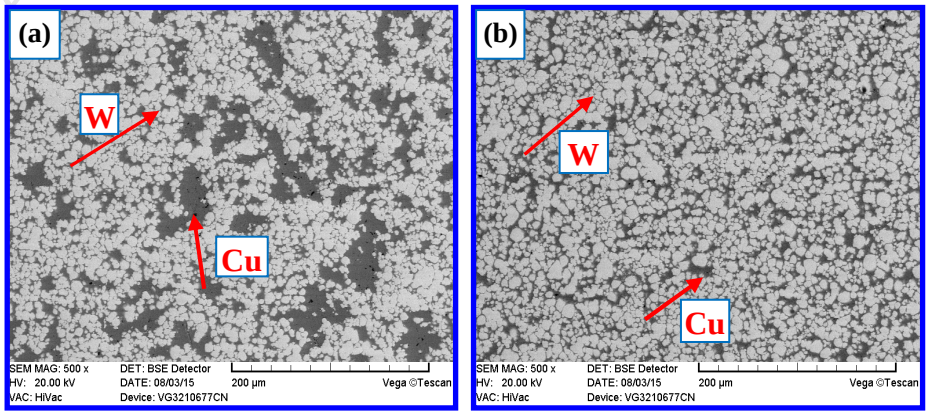

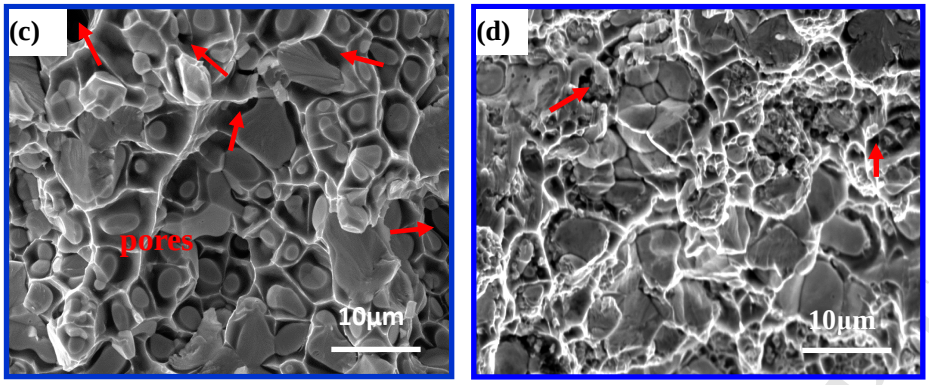

Fig. 5 Microstructure and fracture morphlogy of W70Cu30 alloys prepared with (a),(c) M-Cu-W powders, (b),(d) Cu@W composites powders.

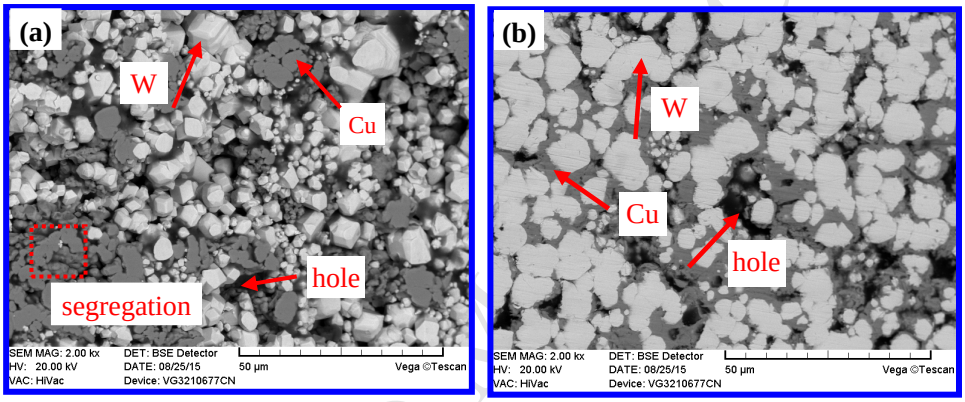

Fig. 6 The morphology of W70Cu30 green compacts (a) M-Cu-W powders, (b) Cu@W composites powders.

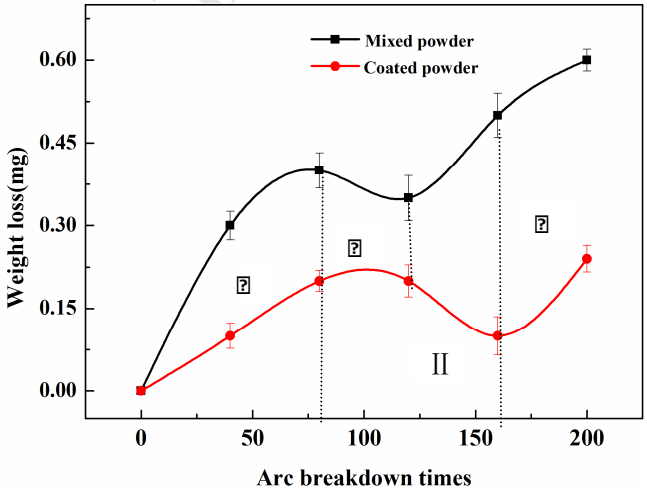

Fig. 7 The curves of arc ablation times and mass accumulated lost of different W70Cu30 alloys.

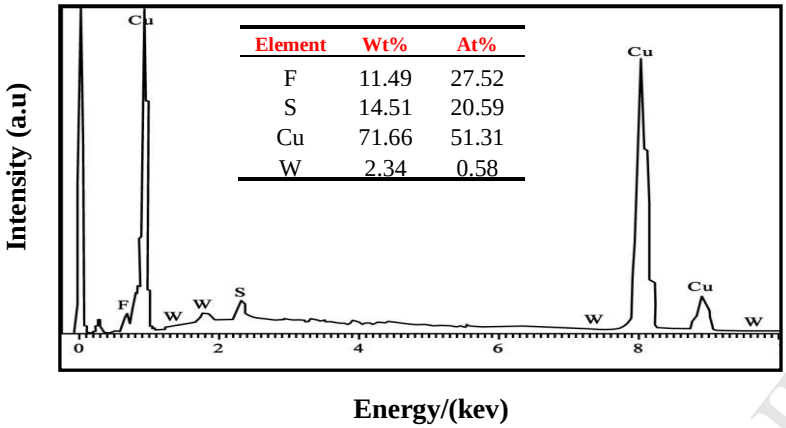

Fig. 8 EDS energy spectrum of W70Cu30 alloy arc breakdown under SF_6 gaseous medium.

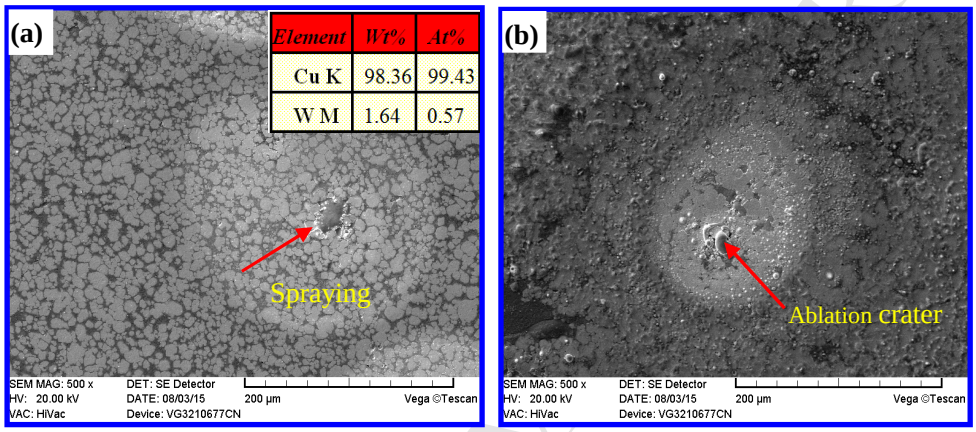

Fig. 9 The surface microstructure after first arc breakdown of W70Cu30 alloy

(a) WCu-C alloy, (b) WCu-M alloy.

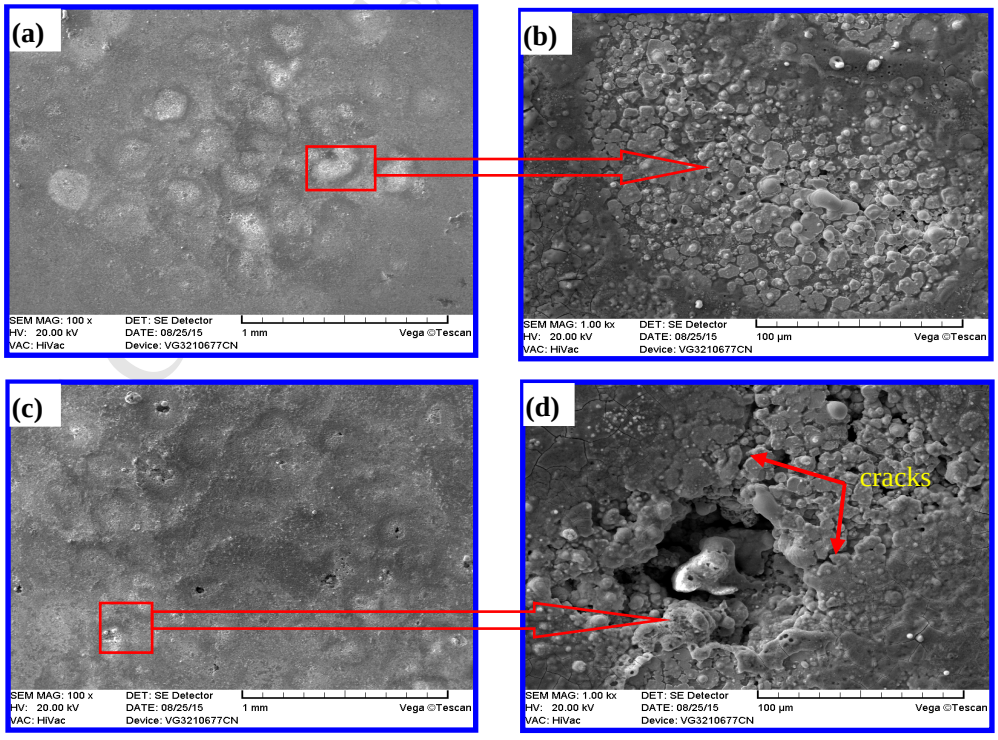

Fig. 10 The surface microstructure after arc breakdown 200 times of W70Cu30 alloy prepared with different powders (a) and (b) WCu-C alloy, (c) and (d) WCu-M alloy.

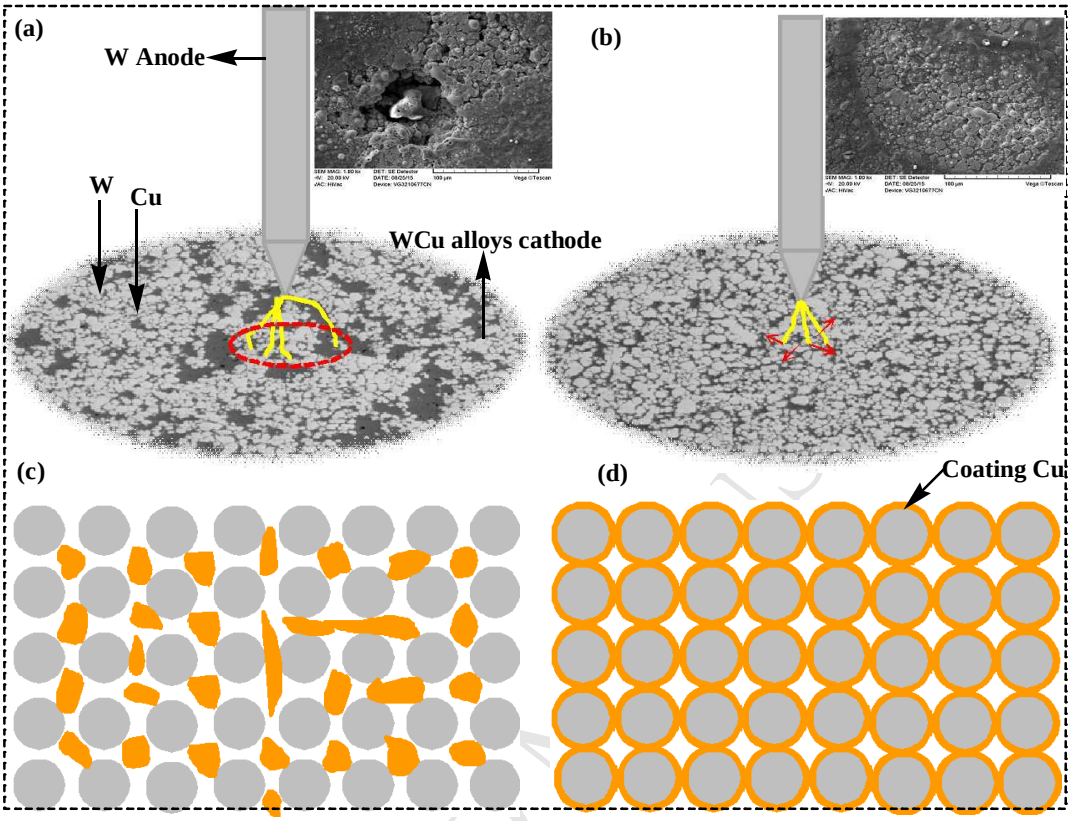

Fig. 11 Schematic illustration of the vacuum breakdown process for WCu alloys.

Table 1 Chemical compositions of W and Cu powders (mass fraction, %).

Powders	W	Cu	Fe	Cr	Ni	Mn
W (wt%)	Bal.	0.05	0.002	＜0.002	-	＜0.005
Cu (wt%)	-	Bal.	0.008	-	＜0.1	＜0.005

Table 2 The compositions of plating solution and reaction conditions.

Chemical	Function	Concentration
$CuSO_4$•$5H_2O$	Source Cu	20g/L
$C_4H_4O_6KNa$•$4H_2O$	Complexing agent	50g/L
$C_{10}H_{14}N_2O_8$•$2H_2O$	Stabilizing agent	5.0mL/L
HCHO	Reducing agent	25mL/L
NaOH	Adjust the pH value	30 wt.%, PH=12

Table 3 The Physical and mechanical properties of W70Cu30 alloy prepared with different composites powders.

Raw material powders	Relative density(%)	Electrical conductivity(IACS %)	Thermal conductivity($W \cdot m^{-1} \cdot K^{-1}$)	Hardness (HV)
Coated powders	99.1	56.4	234	238
Mixing powders	98.0	50.2	210	213
National standard (GB/T8320-2003)	≥96.3	≥42		≥183

Highlights

- The physical properties of WCu-C alloys are much better than WCu-M alloys.
- WCu-C alloys are free of cracks, and show uniformly distribution of W and Cu-Cu.
- WCu-C alloy reveals evaporation of Cu, but WCu-M alloy reveals sputtering of Cu.
- Arc erosion mechanism of WCu-C alloy is Cu-Cu network to disperse arc energy.